BOUNDARY WEIGHT FUNCTIONS FOR CRACKS IN THREE-DIMENSIONAL FINITE BODIES

Chien-Ching Ma * **I-Kuang Shen** **

Department of Mechanical Engineering
National Taiwan University
Taipei, Taiwan 10617, R.O.C.

ABSTRACT

An efficient boundary weight function method for the determination of mode I stress intensity factors in a three-dimensional cracked body with arbitrary shape and subjected to arbitrary loading is presented in this study. The functional form of the boundary weight functions are successfully demonstrated by using the least squares fitting procedure. Explicit boundary weight functions are presented for through cracks in rectangular finite bodies. If the stress distribution of a cut out rectangular cracked body from any arbitrary shape of cracked body subjected to arbitrary loading is determined, the mode I stress intensity factors for the cracked body can be obtained from the predetermined boundary weight functions by a simple integration. Comparison of the calculated results with some solutions by other workers from the literature confirms the efficiency and accuracy of the proposed boundary weight function method.

Keywords : Stress intensity factor, Boundary weight function, Finite body, Through crack.

1. INTRODUCTION

The implementation of damage tolerance analysis for the design of structures containing cracks requires the knowledge of stress intensity factors. Stress intensity factors are now available for a wide range of crack configurations and loadings and have been summarized in well-known handbooks of Tada, *et al.*, [1], Rooke and Cartwright [2] and Sih [3]. It is still found inadequate with regard to the needs in practical applications because actual structural details are often unique so that ready made handbook solutions cannot to be available. There is a great need for simple methods to obtain stress intensity factors for engineering applications with good accuracy.

The weight function concept for two-dimensional elastic crack analysis was first proposed by Bueckner [4], is a powerful and efficient method for determining the stress intensity factor. His weight function satisfy the equations of displacement fields but have a stronger singularity at the crack tip than would be admissible for an actual displacement field. Rick [5] proposed a convenient procedure for weight function determination for plane problems. He showed that weight function could be determined by differentiating known displacement field with respect to crack length. The weight functions serve as a universal function for a given crack geometry and composition; they are independent of applied loading. The weight function concept is, in fact, Green's function of the stress intensity factors for a cracked body. The weight function, once obtained from a single simple load case, can then be used to calculate additional stress intensity factors for the same cracked geometry but with different load conditions. In the original version of the weight function method, the boundary condition dealt with does not involve prescribed displacements. Bowie and Freese [6] have made a reformulation for the weight function to include the mixed traction and displacement boundary condition case. In the study by Bortman and Banks-Sills [7], Rice's displacement derivative definition of the weight function for mode I deformation has been extended to mixed fracture mode.

In recent years, the finite element method applied to fracture mechanics has been well developed. There are several studies that have sought to build up the calculation technique and provide a possible and efficient way to construct the two-dimensional weight functions for finite cracked bodies. Sha [8] used the stiffness derivative technique coupled with singular crack-tip elements to determine the weight functions, and he obtained the two-dimensional weight function for a single edge crack with specified specimen width and length by means of the finite element method. Sha and Yang [9] obtained the two-dimensional weight function for an oblique edge crack by means of the

* Professor ** Graduate student

finite element method using the virtural crack extension technique as suggested by Parks [10] and Hellen [11]. They have extended this method to non-symmetric mixed mode problems and used a special symmetric mesh in the vicinity of the crack tip such that the stress intensity factors for modes I and II could be determined independently. Recently, Tsai and Ma [12] and Ma, Chang and Tsai [13] construct the explicit form of the two-dimensional mixed mode crack face weight function for finite rectangular plates by using the finite element and curve fitting technique. These explicit weight functions are expressed in terms of a position coordinate, crack length, specimen width and length, which are certainly more useful in practical applications. However, the above mentioned crack face weight function method can only be used to determine stress intensity factors for specific cracked geometry.

Because of the computational efficiency, the virtual crack extension technique suggested by Park [10] and Hellen [11] has been widely used in the finite element evaluation of mode I stress intensity factors. The virtual crack extension is a devised algorithm for the efficient calculation of the strain energy release rate of a cracked body. Recently, the use of analytical separation of the crack-tip field into mode I and mode II components with the symmetric mesh in the crack tip neighborhood was proposed by Ishikawa [14] and Sha [15] and Sha and Yang [9]. The method described above is used by Ma, Chang and Tsai [13] for evaluating oblique edge crack and oblique central crack weight function on crack faces for two-dimensional problems. A numerical mode I weight function based upon finite element calculations and the stiffness derivative method has been used for three-dimensional geometries by Banks-Sills and Makevel [16]. By using the principle of superposition, the stress intensity factor under crack-face loading is equivalent to the cracked body with remote loading that produces the same pressure loading on the prospective crack face in the absence of the crack. Hence, for a special regular cracked geometry, only the weight functions on the crack faces are needed for evaluating the stress intensity factors. However, for calculating the stress intensity factors of arbitrary cracked geometries, the usually used crack-face weight function concept will not be a suitable method. In this study, we have introduced the boundary weight function method to calculate the stress intensity factors for arbitrary cracked geometries subjected to general boundary condition on the boundary.

Because of the complexities of the three-dimensional problem in finite crack bodies, no exact solutions of the stress intensity factor are available. There are many techniques which can be used to calculate the stress intensity factor by finite element method, it usually needs a very fine mesh near the crack tip. However, this is not necessary when energy based methods such as virtual crack extension are employed for these calculations. Raju and Newman [17] used the finite element method to obtain the stress intensity factor for a semicircular surface crack in a semi-infinite solid and a semi-elliptical surface crack in a plate of finite thickness. Hechmer and Bloom [18] studied the case of two-symmetric corner cracks emanating from a hole in a plate. In this paper, an efficient method which combines finite element with boundary weight functions has been established in determining stress intensity factors in three-dimensional configuration and subjected to arbitrary loadings for finite cracked body. The boundary weight function method has also been investigated by Ma, *et al.*, [19] for two-dimensional case and we will extend this methodology to three-dimensional analogy in the study. Three-dimensional problems are much more difficult than two-dimensional problems, since a weight function exists for every point along the crack front. The stress intensity factor for any specific crack geometry subjected to general prescribed boundary conditions as shown in Fig. 1 is equal to that of the cut out rectangular cracked body (Fig. 2) with the same stress distribution on the cut out rectangular boundary (dash line) on Fig. 1. The stress distribution on the cut out rectangular boundary can be obtained with accuracy with an ordinary finite element mesh. Which means that we need not to use very fine mesh near the crack tip in order to get good results of the stress distribution on the cut out rectangular boundary. Once we have obtained the value of boundary weight function for the rectangular cracked geometry, the stress intensity factor under any load can be calculated by a simple surface integration. In this study, these boundary weight functions are expressed in terms of the nondimensional quantities of position coordinate on the boundary. The cracked geometry to be considered in this study is a through straight crack in a rectangular finite body. These explicit weight functions are then used to calculate the stress intensity factors for some specific crack problems and are compared with known results in the literature.

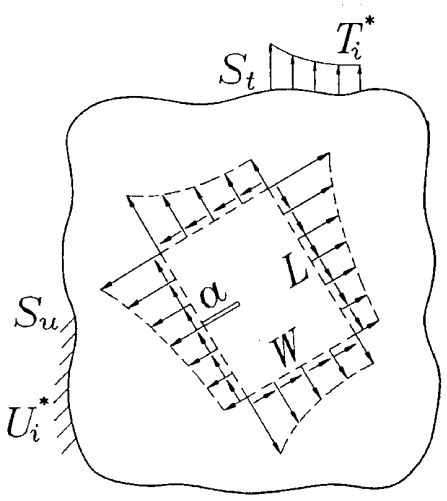

Fig. 1 Configuration for a arbitrary cracked body subjected to general boundary condition with a cut rectangular cracked body contains an edge through crack

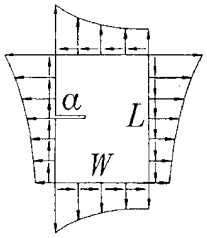

Fig. 2 Geometry of a rectangular cracked body with an edge through crack as indicated in Fig. 1

2. WEIGHT FUNCTION FORMULATION AND NUMERICAL TECHNIQUE

The weight function method as presented by Bueckner [4] and Rice [5] was used to compute mode I stress intensity factor of symmetric cracked bodies with symmetric loading. Bowie and Freese [6] and Bortman and Banks-Sills [7] extended Rice's displacement derivative definition of the weight function for two-dimensional mode I deformation to mixed fracture mode and mixed boundary conditions. The two-dimensional stress intensity factor is expressed as a product of the applied load and the weight function as follows,

$$K_I = \int_{S_t} \mathbf{t}^* \cdot \mathbf{h}_\mathbf{I} \, ds + \int_{S_u} \mathbf{u}^* \cdot \mathbf{h}_\mathbf{I}^\mathbf{u} \, ds \tag{1}$$

$$K_{II} = \int_{S_t} \mathbf{t}^* \cdot \mathbf{h}_\mathbf{II} \, ds + \int_{S_u} \mathbf{u}^* \cdot \mathbf{h}_\mathbf{II}^\mathbf{u} \, ds \tag{2}$$

The decoupled weight function vectors for mode I and mode II in two-dimensional configuration can be represented as follows

$$\mathbf{h}_\mathbf{I} = \frac{H}{2K}\left(K_{II}^{(2)} \frac{\partial \mathbf{u}^{(1)}}{\partial a} - K_{II}^{(1)} \frac{\partial \mathbf{u}^{(2)}}{\partial a} \right) \tag{3}$$

$$\mathbf{h}_\mathbf{I}^\mathbf{u} = -\frac{H}{2K}\left(K_{II}^{(2)} \frac{\partial \mathbf{t}^{(1)}}{\partial a} - K_{II}^{(1)} \frac{\partial \mathbf{t}^{(2)}}{\partial a} \right) \tag{4}$$

$$\mathbf{h}_\mathbf{II} = \frac{H}{2K}\left(K_{I}^{(1)} \frac{\partial \mathbf{u}^{(2)}}{\partial a} - K_{I}^{(2)} \frac{\partial \mathbf{u}^{(1)}}{\partial a} \right) \tag{5}$$

$$\mathbf{h}_\mathbf{II}^\mathbf{u} = -\frac{H}{2K}\left(K_{I}^{(1)} \frac{\partial \mathbf{t}^{(2)}}{\partial a} - K_{I}^{(2)} \frac{\partial \mathbf{t}^{(1)}}{\partial a} \right) \tag{6}$$

and

$$K = K_I^{(1)} K_{II}^{(2)} - K_I^{(2)} K_{II}^{(1)} \neq 0$$

in which $H = E$ (Young's modulus) for generalized plane stress and $H = E / (1 - \nu^2)$ for plane strain, ν being Poisson's ratio. The subscript **I** in $\mathbf{h}_\mathbf{I}$ is used to denote the mode I weight function. The boundary has been divided into the part for specified traction S_t and that for specified displacement S_u. Configurations "(1)" and "(2)" are geometrically equivalent to the original problem. The corresponding stress intensity factors and displacement vectors will be denoted by $K_{I(II)}^{(1)}$, $\mathbf{u}^{(1)}$ and $K_{I(II)}^{(2)}$, $\mathbf{u}^{(2)}$, respectively. Once the weight functions are determined from the solution for any particular load system, the two-dimensional stress intensity factor induced by any other load system can be obtained from Eqs. (1) and (2).

The weight function method also applies to three-dimensional problems of cracked bodies. Three-dimensional problems are much more difficult than two-dimensional problems since a weight function exists for every point along the crack front. Consider a plane crack in a solid with a front of smooth shape, and both the body and load systems under consideration being symmetrical about the plane of the crack. A three-dimensional weight function may be defined as [5,20]

$$h(P, P') = \frac{H}{2\,K^*(P')} \frac{\delta U(P)}{\delta A(P')} \tag{7}$$

where P is a load point, P' is a point along the crack front. $\delta A(P')$ is a small extension of the crack surface at P' and $K^*(P')$ is the stress intensity factor at point P' under special loading. This expression is the general definition of three-dimensional weight functions. This is also an unique function of P and P' for a given cracked body geometry and composition, and is completely independent of the way in which the body is loaded. For an arbitrary symmetric load system $t(P)$ applied on the cracked body, the stress intensity factor at P' can be obtained from integration as follow

$$K(P') = \int_s t(P)\, h(P, P')\, dA(P) \tag{8}$$

However, by employing the linear superposition method proposed in this study, only the weight functions along the prospective boundaries of rectangular cracked body are of primary interest for evaluating the stress intensity factor.

As indicated in (7), one needs an efficient means for solving the reference geometry fracture mechanics problem to obtain the rate of change in boundary displacements and stress intensity factors. Unfortunately, the exact solution of displacement field is available only for very few ideal crack problems. An efficient finite element method for determining both the stress intensity factors and weight functions for cracked body of interest has been achieved by combining the singular crack-tip elements with the virtual crack extension technique.

Consider a cracked body with general boundary condition applied on the boundary as shown in Fig. 1, which will induce normal and shear stresses along a regular specified rectangular boundary. The stress intensity factors of the original problem is equal to that of the cut out regular rectangular cracked body with through crack subjected to equal stress distribution on the rectangular boundary of Fig. 1. Hence the problem for the case of a rectangular body with an edge through crack shown in Fig. 2 is of special interest. Once the weight functions along the rectangular boundary are determined, the stress intensity factors can be easily obtained by simple integrations over the distributed stress and the boundary weight function.

3. BOUNDARY WEIGHT FUCNTIONS FOR FINITE CRACKED BODIES

In order to determine the boundary weight functions, reference stress intensity factor together with the displacement field on boundaries must be known. Exact solutions of the displacement field are available for only a very few crack problems. For most cases of practical interest, exact solutions hardly exist. Hence, good approximations to the displacement field for such cases are very useful for constructing the explicit form of weight function. The evaluation of the weight function requires the calculation of both the stress intensity factor and the displacement derivatives. For specimens with finite dimension, the calculations are usually done by finite element method. Because of the invariant characteristics with respect to the loading conditions for a given geometry and constraint conditions, the simplest uniformly distributed loading is used for the finite element evaluation of the explicit weight functions for boundaries of interest. The finite element evaluation of the weight functions using the virtual crack extension technique coupled with singular elements is used in this study.

The conventional determination of the two-dimensional weight function by several authors [8,12,13] has usually been restricted to crack face only, since the stress intensity factor under crack face loading is equivalent to load the cracked body with remote loading that produces the same pressure loading on the prospective crack face in the absence of the crack. However, the crack face weight function will behave singularity near the crack tip which should be carefully analyzed to get accurate result. Therefore the nonsingular boundary weight function is used in this study.

In this study, the weight functions for cracked rectangular body are investigated for calculating the stress intensity factor of arbitrary cracked bodies subjected to general boundary conditions. The standard three-dimensional twenty-nodal serendipity element of quadratic form are used. The elements in the vicinity of the crack front are modeled with the degenerated quarter-point quadratic element as shown in Fig. 3. The dash line shown in Fig. 4 represents the virtual crack extension near the crack front.

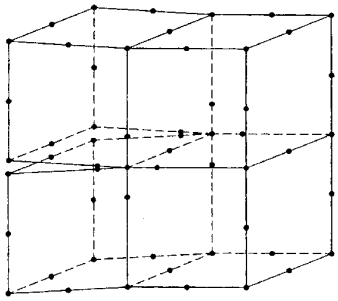

Fig. 3 The quarter-point quadratic isoparametric element at the crack front

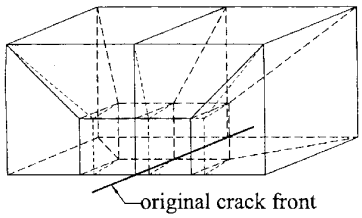

Fig. 4 The virtual crack extension near the crack front

The rectangular cracked body has five boundaries and the boundary weight function expressed as a function of the X-Y plane is taken to have the following polynomial form

$$\sqrt{a^3}\, h(X/l, Y/l) = \sum_{n=1}^{6} \sum_{m=1}^{6} C_{nm} (X/W)^n (Y/L)^m \quad (9)$$

The corresponding boundary weight functions for boundaries on Y-Z and X-Z planes have the similar form as (9). The corresponding configuration for a through crack in a rectangular body is represented in Fig. 5. The numerical results of the boundary weight functions are calculated by using the finite element method. Since the weight function is universal and is independent of the loading system, the most simple loading system of uniformly distributed tensile loading applied on the top surface is chosen for the numerical calculation. The stress intensity factor for uniformly distributed tensile loading is obtained by using the nodal-force method proposed by Raju and Newman [17]. The nodal forces normal to the crack plane and ahead of the crack front are used to calculate the stress intensity factor. The advantage of this method is that it requires no prior assumption of either plane stress or plane strain condition. For a through crack in a finite body, the state of stress varies from plane strain in the interior to plane stress at the free surface. The numerical results form the basic data for curve fitting. By using least squares procedure, the discretized values of the boundary weight functions are approximated with (9). The tabulation of the coefficients C_{nm} for different crack geometries are given in Tables 1 and 2. Because of the

Table 1 The interpolation coefficients C_{nm} of the boundary weight function for a point at the crack tip $Z = T/2$ of a rectangular body with a through crack ($W:L:T = 1:1:0.5$, $a/W = 1/2$) subjected to symmetric loading

	C_{nm}	1	2	3	4	5	6
top in normal *Y*-direction	1	.22734564D+02	−.14447874D+00	.36890891D+01	−.13600398D+02	.13600014D+02	.51216241D−03
	2	−.30950416D+02	.34973741D+01	−.70187776D+02	.25277484D+03	−.25278467D+03	.14076406D−01
	3	.16472267D+02	−.71435182D+02	.94851055D+03	−.32225936D+04	.32227067D+04	−.15987253D+00
	4	−.90545090D+02	.31422403D+03	−.27647948D+04	.85454885D+04	−.85458356D+04	.48932491D+00
	5	.14805923D+03	−.43899964D+03	.29749729D+04	−.83880151D+04	.83884260D+04	−.57892304D+00
	6	−.69231495D+02	.19250157D+03	−.10884618D+04	.28138838D+04	−.28140508D+04	.23516517D+00
top in shear *X*-direction	1	.11282438D+02	.17600093D+00	.23327184D+01	−.10738819D+02	.10738532D+02	.40182169D−03
	2	−.22772753D+01	−.44683478D+01	.44439805D+02	−.14201849D+03	.14203919D+03	−.29344547D−01
	3	.21726350D+02	.99670173D+02	−.10348697D+04	.33421686D+04	−.33423432D+04	.24721583D+00
	4	−.62936005D+02	−.33833506D+03	.34242042D+04	−.10990282D+05	.10990778D+05	−.70120255D+00
	5	.54432067D+02	.39394263D+03	−.39014412D+04	.12454390D+05	−.12454957D+05	.80061163D+00
	6	−.13410515D+02	−.15209656D+03	.14743790D+04	−.46808098D+04	.46810347D+04	−.31781056D+00
top in shear *Z*-direction	1	.87180916D+00	.16080710D+00	−.46816645D+01	.35391875D+02	−.87448966D+02	.69959176D+02
	2	−.14224614D+00	.24456757D+01	.38839834D+02	−.38578590D+03	.10019986D+04	−.80159913D+03
	3	−.31521835D+00	−.40679489D+02	−.35508511D+03	.45182963D+04	−.12134551D+05	.97076423D+04
	4	−.14858033D+02	.17602195D+03	.10486126D+04	−.13052497D+05	.34963045D+05	−.27970441D+05
	5	.31863603D+02	−.24115375D+03	−.11997885D+04	.14146285D+05	−.37639706D+05	.30111770D+05
	6	−.16614361D+02	.10336717D+03	.46473715D+03	−.51942874D+04	.13723916D+05	−.10979135D+05
right side in normal *X*-direction	1	−.13025619D−03	.11796798D+01	−.23247510D+01	.22901475D+01	−.11450864D+01	.10039673D−04
	2	−.20336424D−01	−.15335516D+00	.10843278D+01	−.17836156D+01	.75625998D+00	.96378450D−01
	3	.58146957D+01	−.37003193D+01	.78424856D+01	−.89375184D+01	.55991596D+01	−.80379320D+00
	4	−.67060197D+00	−.21371981D+00	−.46480218D+00	.31864336D+01	−.47592182D+01	.22512839D+01
	5	−.39504896D+01	.57333884D+01	−.13710022D+02	.13862255D+02	−.33123127D+01	−.25732915D+01
	6	.19323944D+01	−.29733380D+01	.80690386D+01	−.93549285D+01	.32298091D+01	.10294137D+01
right side in shear *Y*-direction	1	.17950118D−03	−.52693352D−04	−.19643738D−02	.40342043D−02	−.20172183D−02	.81131145D−07
	2	−.26293333D+01	−.52293773D+00	.35075962D+01	−.73594419D+01	.60857074D+01	−.17109239D+01
	3	−.34679355D+00	−.28921856D+01	.13104503D+02	−.88403311D+01	−.15629588D+02	.14257602D+02
	4	.44876673D+01	.88956009D+01	−.42805908D+02	.35384674D+02	.38446771D+02	−.39921139D+02
	5	−.35512320D+01	−.75560796D+01	.35475041D+02	−.18768357D+02	−.54774657D+02	.45624055D+02
	6	.82480651D+00	.19440779D+01	−.86924630D+01	−.13310327D+01	.26329010D+02	−.18249593D+02
right side in shear *Z*-direction	1	−.59254278D−04	.80071948D+00	.23480398D+00	−.25874160D+01	.36463205D+01	−.14585287D+01
	2	.51452405D−01	−.52670374D+00	.21266505D+01	−.42686136D+01	.42762685D+01	−.17105053D+01
	3	.35837411D+00	.43070021D+00	−.10814695D+02	.31784313D+02	−.36861788D+02	.14744721D+02
	4	.12345513D+01	−.66323896D+01	.17124627D+02	−.26865690D+02	.23173964D+02	−.92696172D+01
	5	−.24293755D+01	.10675518D+02	−.12623947D+02	−.76718189D+01	.24131604D+02	−.96525989D+01
	6	.10750171D+01	−.47888784D+01	.37560435D+01	.11364245D+02	−.20802381D+02	.83209344D+01
left side in normal *X*-direction	1	−.12187572D+01	−.34574087D−01	.33043527D−01	.30639992D−02	−.15370488D−02	.31464407D−05
	2	.51845109D+01	−.13948986D−01	−.11976732D+01	.36523723D+01	−.39535350D+01	.15127836D+01
	3	−.23834128D−01	.15733767D+01	−.72435884D+01	.10974615D+01	.17179501D+02	−.12606746D+02
	4	−.38803871D+00	−.31213493D+01	.27446427D+02	−.19969570D+02	−.39654712D+02	.35299196D+02
	5	.81085249D+00	.21834855D+01	−.28968144D+02	.20791268D+02	.46335592D+02	−.40342196D+02
	6	−.38598905D+00	−.50193852D+00	.99011849D+01	−.56871982D+01	−.19849009D+02	.16136960D+02
left side in shear *Y*-direction	1	.80050280D+01	.11551779D+00	.21086552D+00	−.65277898D+00	.32640763D+00	−.12129590D−04
	2	.17668361D−01	.44289323D+00	−.22599789D+01	.18436285D+01	.21771730D+01	−.22037139D+01
	3	−.95246545D−01	−.41947644D+01	.21905256D+02	−.20500160D+02	−.15574197D+02	.18363854D+02
	4	.54552595D+00	.84069241D+01	−.50159546D+02	.41727928D+02	.51442453D+02	−.51417732D+02
	5	−.73139529D+00	−.68175266D+01	.44826912D+02	−.28274080D+02	−.68497589D+02	.58762258D+02
	6	.29561804D+00	.20312120D+01	−.14274605D+02	.53891515D+01	.30358895D+02	−.23504645D+02
left side in shear *Z*-direction	1	.330814505D+00	−.22725943D−01	.20934857D+00	−.86863916D+00	.10936117D+01	−.43744542D+00
	2	−.12062778D+00	−.52977802D−01	−.36810157D−01	.30895981D+01	−.45976052D+01	.18390502D+01
	3	−.18704587D+00	.86493160D−01	−.20284086D+01	.10989573D+02	−.14455928D+02	.57823642D+01
	4	.11653618D+01	.71284224D+00	−.32717258D+01	−.17348781D+02	.29294970D+02	−.11718032D+02
	5	−.13925609D+01	−.15326814D+01	.13450336D+02	−.10623195D+02	.24842999D+01	−.99363689D+00
	6	.51455849D+00	.81047949D+00	−.85106669D+01	.15646637D+02	−.14959211D+02	.59836445D+01
ahead side in normal *Z*-direction	1	.10066096D+01	−.11675704D+01	−.57831988D+01	.56462180D+02	−.12990936D+03	.94633799D+02
	2	−.13334011D+00	−.58323289D+02	.14542189D+04	−.84052052D+04	.18420655D+05	−.13924415D+05
	3	−.32618982D+02	.67982589D+03	−.13082759D+05	.73712485D+05	−.16065767D+06	.12130994D+06
	4	.23776044D+03	−.28259463D+04	.36136505D+05	−.19035702D+06	.40840159D+06	−.30740584D+06
	5	−.41165796D+03	.44283321D+04	−.43040992D+05	.20835841D+06	−.43506669D+06	.32444541D+06
	6	.20772882D+03	−.22781575D+04	.19059359D+05	−.85465132D+05	.17291442D+06	−.12720338D+06
ahead side in shear *X*-direction	1	−.35470409D+01	.33238535D+02	−.28277070D+02	.74404138D+02	−.77517030D+02	.26353606D+02
	2	.72920744D+01	−.41921031D+03	.36543406D+04	−.13393144D+05	.22838105D+05	−.14937447D+05
	3	−.63791426D+02	.38517780D+04	−.34652954D+05	.13008081D+06	−.22576895D+06	.14955062D+06
	4	.16769916D+03	−.10429543D+05	.97379260D+05	−.37464767D+06	.65932546D+06	−.43961807D+06
	5	−.15347637D+03	.10790825D+05	−.10550098D+06	.41598648D+06	−.74131441D+06	.49671201D+06
	6	.45352147D+02	−.38140209D+04	.39095795D+05	−.15763557D+06	.28391953D+06	−.19092835D+06
ahead side in shear *Y*-direction	1	.22531951D+02	−.96020053D+00	.17136944D+02	−.60515447D+02	.80290133D+02	−.33781897D+02
	2	−.35187019D+02	.33735217D+03	−.41667947D+04	.19040087D+05	−.37230276D+05	.26377222D+05
	3	.15404083D+03	−.36646275D+04	.39550939D+05	−.17688249D+06	.34507897D+06	−.24484789D+06
	4	−.81710176D+03	.12646083D+05	−.11997820D+06	.52219710D+06	−.10131191D+07	.71831957D+06
	5	.12936322D+04	−.17159955D+05	.15021549D+06	−.63822970D+06	.12288759D+07	−.86881678D+06
	6	−.62325063D+03	.79692232D+04	−.66964071D+05	.27949273D+06	−.53408284D+06	.37619825D+06
behind side in normal *Z*-direction	1	.70869445D+00	.35257340D+01	−.16050520D+02	.31735629D+02	−.31548996D+02	.15107927D+02
	2	.61220128D+01	−.10962219D+03	.10528988D+03	.20541872D+04	−.66808902D+04	.58669138D+04
	3	−.24247006D+02	.91181939D+03	−.17031835D+04	−.13427222D+05	.49067166D+05	−.44615404D+05
	4	−.52277448D+02	−.23605453D+04	.12053881D+05	−.62369433D+04	−.44249764D+05	.56959201D+05
	5	.16723655D+03	.24011529D+04	−.20423515D+05	.50654450D+05	−.44945768D+05	.58516387D+04
	6	−.95985173D+02	−.84205790D+03	.99389628D+04	−.32926257D+05	.46589943D+05	−.23904975D+05
behind side in shear *X*-direction	1	−.35657963D+01	.33772148D+02	−.33221576D+02	.94391244D+02	−.11412764D+03	.51249987D+02
	2	.86459591D+01	−.45721834D+03	.40075926D+04	−.14832827D+05	.25501014D+05	−.16766080D+05
	3	−.76647081D+02	.42119188D+04	−.38001084D+05	.14374039D+06	−.25106665D+06	.16694498D+06
	4	.20963054D+03	−.11602906D+05	.10828849D+06	−.41917561D+06	.74184094D+06	−.49638913D+06
	5	−.20873111D+03	.12335702D+05	−.11986482D+06	.47463473D+06	−.85004396D+06	.57155207D+06
	6	.70613091D+02	−.45197666D+04	.45657811D+05	−.18443659D+06	.33362597D+06	−.22515567D+06
behind side in shear *Y*-direction	1	.70869445D+00	.35257340D+01	−.16050520D+02	.31735629D+02	−.31548996D+02	.15107927D+02
	2	.61220128D+01	−.10962219D+03	.10528988D+03	.20541872D+04	−.66808902D+04	.58669138D+04
	3	−.24247006D+02	.91181939D+03	−.17031835D+04	−.13427222D+05	.49067166D+05	−.44615404D+05
	4	−.52277448D+02	−.23605453D+04	.12053881D+05	−.62369433D+04	−.44249764D+05	.56959201D+05
	5	.16723655D+03	.24011529D+04	−.20423515D+05	.50654450D+05	−.44945768D+05	.58516387D+04
	6	−.95985173D+02	−.84205790D+03	.99389628D+04	−.32926257D+05	.46589943D+05	−.23904975D+05

Table 2 The interpolation coefficients C_{nm} of the boundary weight function for a point at the crack tip $Z = T/4$ of a rectangular body with a through crack ($W:L:T = 1:1:0.5$, $a/W = 1/2$) subjected to symmetric loading

	C_{nm}	1	2	3	4	5	6
top in normal *Y*-direction	1	.28293755D+02	−.25931974D+02	.12413690D+02	−.73494698D+02	.16815320D+03	−.13075637D+03
	2	−.33198318D+02	.23333966D+02	−.14118152D+03	.74399925D+03	−.16241260D+04	.12182918D+04
	3	.55582493D+02	−.22556275D+03	.93935368D+03	−.45414896D+04	.94806208D+04	−.66689977D+04
	4	−.21662556D+03	.77273341D+03	−.25086920D+04	.10997153D+05	−.21979274D+05	.14526274D+05
	5	.27383972D+03	−.87362564D+03	.26508414D+04	−.10681954D+05	.20481193D+05	−.12648933D+05
	6	−.10952140D+03	.31973067D+03	−.94507733D+03	.35834455D+04	−.66449916D+04	.38058663D+04
top in shear *X*-direction	1	.11217605D+02	−.14174551D+01	.73955229D+01	−.46267044D+02	.98059515D+02	−.68736487D+02
	2	−.25879689D+01	.33923229D+01	−.63684846D+02	.45783067D+03	−.11905328D+04	.10262303D+04
	3	.21286978D+02	.12116509D+02	.31420779D+03	−.32225836D+04	.94436009D+04	−.87111178D+04
	4	−.40664554D+02	.98919910D+02	−.28418121D+04	.15994828D+05	−.39023176D+05	.34116653D+05
	5	.14415961D+02	−.25278915D+03	.50699352D+04	−.24501282D+05	.55023140D+05	−.46459877D+05
	6	.58488663D+01	.13684676D+03	−.24699638D+04	.11180954D+05	−.24025350D+05	.19857376D+05
top in shear *Z*-direction	1	.62035224D+01	−.24546848D+00	.13973748D+01	−.59825687D+01	.10527991D+02	−.57719073D+01
	2	−.78830656D+00	.76662702D+01	.39007522D+02	−.35466175D+03	.84446106D+03	−.66503678D+03
	3	.20517591D+02	−.92026092D+02	−.39799683D+03	.40740790D+04	−.99542890D+04	.78228743D+04
	4	−.85720107D+02	.31039556D+03	.13437237D+04	−.13157332D+05	.31660201D+05	−.24425855D+05
	5	.10215289D+03	−.37092835D+03	−.17808565D+04	.16109839D+05	−.37784803D+05	.28514261D+05
	6	−.37984809D+02	.14507237D+03	.79160315D+03	−.66251339D+04	.15111224D+05	−.11147778D+05
right side in normal *X*-direction	1	.11015292D−03	.10839470D+01	−.24951991D+01	.40032176D+01	−.36580145D+01	.10658592D+01
	2	−.42665685D−01	.12214542D−01	.17480137D+01	−.75711618D+01	.10692377D+02	−.48366168D+01
	3	.68330334D+01	−.62226489D+01	.67323433D+01	.82782418D+01	−.28160101D+02	.17409969D+02
	4	−.25327030D+01	.67596480D+01	−.94132423D+01	−.14432724D+02	.52159355D+02	−.32039189D+02
	5	−.24548843D+01	−.26041092D+01	.10918781D+02	−.70490193D+01	−.20910121D+02	.17441765D+02
	6	.15441453D+01	.59604768D+00	−.68996895D+01	.12697118D+02	−.48779021D+01	−.99626234D+00
right side in shear *Y*-direction	1	.19796920D−03	−.11472578D−02	.24984042D−02	.31566047D−03	−.45908181D−02	.28937643D−02
	2	−.14044025D+01	−.52881328D+01	.13639740D+02	−.22716373D+02	.17297294D+02	−.52939871D+01
	3	−.30716898D+00	.93029207D+00	−.89867860D+01	.26450300D+02	−.31759298D+02	.13401428D+02
	4	.39502381D+01	.67522234D+01	−.18954752D+02	.74830382D+01	.20790165D+02	−.15383418D+02
	5	−.42755375D+01	−.37338213D+01	.17102309D+02	−.53885100D+01	−.21006987D+02	.14803453D+02
	6	.14594608D+01	−.26226539D+00	−.25112239D+01	−.33449592D+01	.10450825D+02	−.56973054D+01
right side in shear *Z*-direction	1	−.22109821D−03	.42969109D+00	.48002703D+00	−.22468073D+01	.33676539D+01	−.14013215D+01
	2	.20297160D−01	.40150155D+00	−.23845675D+01	.26747094D+01	.77200487D+00	−.15150569D+01
	3	.27531905D+01	−.46993752D+01	.16638381D+02	−.38088949D+01	−.33793483D+02	.24427919D+02
	4	.43946376D+00	.64832546D+01	−.44417186D+02	.25814720D+02	.70268921D+02	−.59324464D+02
	5	−.30830462D+01	−.22460526D+01	.50154827D+02	−.42225486D+02	−.66576863D+02	.64513316D+02
	6	.14179362D+01	−.39324839D+00	−.20568091D+02	.21027738D+02	.24161651D+02	−.25970312D+02
left side in normal *X*-direction	1	−.90461145D+00	−.31594150D+00	.72430833D−01	−.72507031D+00	.91025238D+00	−.33686682D+00
	2	.46879476D+01	.41165969D+00	−.16733561D+01	.49560362D+01	−.47758944D+01	.14156066D+01
	3	−.77554583D+00	−.35580870D+00	.78722249D+01	−.10959739D+02	.29282045D+01	.15891223D+01
	4	.23004930D+01	.17747706D+01	−.18568253D+02	.12052055D+02	.14208595D+02	−.12555754D+02
	5	−.17919749D+01	−.35601062D+01	.20862444D+02	−.10410972D+02	−.20112667D+02	.15726372D+02
	6	.43706507D+00	.18765026D+01	−.83481128D+01	.39789006D+01	.81696129D+01	−.63354221D+01
left side in shear *Y*-direction	1	.99333425D+01	−.44298977D+01	.31816792D+00	−.85765959D+00	.97875435D+00	−.40593352D+00
	2	.10223805D−01	−.88072568D+00	.48985278D+01	−.10151073D+02	.93428196D+01	−.32120490D+01
	3	.58400106D−01	.42869177D+01	−.20978665D+02	.36188343D+02	−.27876009D+02	.82633511D+01
	4	.30605673D+00	−.70106841D+01	.25767690D+02	−.27468204D+02	.38533716D+01	.48347571D+01
	5	−.56537236D+00	.49323306D+01	−.10078190D+02	−.11172232D+02	.37951294D+02	−.21446031D+02
	6	.24637157D+00	−.13084699D+01	.13538364D+00	.12817794D+02	−.23337538D+02	.11600745D+02
left side in shear *Z*-direction	1	−.22359341D+01	.22824784D−01	−.25476575D+00	.46368958D+00	−.28683711D+00	.45367209D−01
	2	.44274854D+01	−.30601511D+00	.61143398D+00	.99366811D−01	−.97002362D+00	.56874303D+00
	3	.33801653D+00	.10586712D+01	.16316106D+01	−.60121626D+01	.37434720D+01	−.32819835D+00
	4	−.74473222D+00	−.23167305D+01	−.53319831D+01	.12260361D+02	−.13168879D+01	−.37354952D+01
	5	.45390441D+00	.26091023D+01	.36489365D+01	−.77702820D+01	−.36502975D+01	.57664645D+01
	6	−.50852344D−01	−.10648011D+01	−.35744770D+00	.95707608D+00	.25644855D+01	−.23635382D+01
ahead side in normal *Z*-direction	1	−.62600343D+01	.22106171D+02	.55028306D+01	.76872555D+02	−.30094398D+03	.29570997D+03
	2	.12736150D+02	.31357811D+03	−.31020170D+04	.99901228D+04	−.13610754D+05	.66231380D+04
	3	−.20386043D+03	−.14533881D+04	.21845227D+05	−.82528923D+05	.13136320D+06	−.76917916D+05
	4	.92932140D+03	−.17630695D+04	−.27931317D+05	.14879330D+06	−.28321752D+06	.19040185D+06
	5	−.13490641D+04	.82988997D+04	−.10228000D+05	−.46060471D+05	.15703176D+06	−.13430474D+06
	6	.62221733D+03	−.55574319D+04	.20718264D+05	−.35431466D+05	.18148666D+05	.74593041D+04
ahead side in shear *X*-direction	1	−.26266064D+01	.31587535D+02	−.51901143D+02	.20108005D+03	−.31825496D+03	.18501746D+03
	2	.61542415D−01	−.38831463D+03	.48670201D+04	−.22643413D+05	.45538766D+05	−.33315282D+05
	3	.32631578D+02	.21442676D+04	−.35186427D+05	.18221265D+06	−.38675014D+06	.29150503D+06
	4	−.18127502D+03	−.20135398D+04	.71282483D+05	−.43078035D+06	.97021143D+06	−.75094564D+06
	5	.30957479D+03	−.20186640D+04	−.48769640D+05	.38258871D+06	−.92977274D+06	.74231002D+06
	6	−.16041239D+03	.23036433D+04	.74036839D+04	−.10952331D+06	.29712820D+06	−.24697015D+06
ahead side in shear *Y*-direction	1	.28331374D+02	−.90787577D+01	.13515181D+03	−.68515128D+03	.14292921D+04	−.10555079D+04
	2	−.74878355D+02	.59339367D+03	−.71959874D+04	.37358801D+05	−.80405750D+05	.60798067D+05
	3	.63325723D+03	−.64170790D+04	.62095954D+05	−.30362961D+06	.64165679D+06	−.48148199D+06
	4	−.24325861D+04	.23326860D+05	−.18602374D+06	.82801006D+06	−.16813930D+07	.12368910D+07
	5	.32996094D+04	−.32634433D+05	.23533692D+06	−.96813256D+06	.18841179D+07	−.13533747D+07
	6	−.14633969D+04	.15391882D+05	−.10674132D+06	.41694111D+06	−.78382091D+06	.55098247D+06
behind side in normal *Z*-direction	1	−.64406292D+01	.26645061D+02	−.10409276D+02	.45138029D+02	−.10407145D+03	.87801488D+02
	2	.84765100D+01	−.57251763D+02	.16438969D+03	−.27847353D+03	.40162146D+03	−.34505976D+03
	3	−.55782708D+02	.64887435D+03	−.27097551D+04	.61097725D+04	−.81458179D+04	.51436735D+04
	4	.15653511D+03	−.25072998D+04	.14015721D+05	−.40738811D+05	.61977190D+05	−.38777445D+05
	5	−.14184482D+03	.32564125D+04	−.21461243D+05	.68421726D+05	−.10883092D+06	.68572281D+05
	6	.40769984D+02	−.13667818D+04	.10008327D+05	−.33515731D+05	.54581857D+05	−.34591316D+05
behind side in shear *X*-direction	1	−.37429981D+01	.30485827D+02	−.11990418D+02	.34039238D+02	−.54022845D+02	.37601417D+02
	2	.57133685D+01	−.20527427D+03	.14527802D+04	−.45456296D+04	.69465862D+04	−.42927855D+04
	3	−.57056947D+02	.20444383D+04	−.14327802D+05	.44378132D+05	−.67253068D+05	.41403169D+05
	4	.16426507D+03	−.61752110D+04	.44338366D+05	−.14073605D+06	.21807748D+06	−.13676872D+06
	5	−.16764191D+03	.69936665D+04	−.52241509D+05	.17073327D+06	−.27038953D+06	.17179694D+06
	6	.58442979D+02	−.26877670D+04	.20841481D+05	−.69828603D+05	.11239953D+06	−.71933923D+05
behind side in shear *Y*-direction	1	.15443333D+02	.36788853D+01	−.35355388D+02	.16442494D+03	−.33861207D+03	.25077914D+03
	2	−.16285937D+02	−.79730706D+02	.18856453D+03	−.17971209D+03	.80948382D+02	−.27705887D+02
	3	−.79946981D+02	.60155968D+03	−.94078034D+03	−.29226397D+04	.10396924D+05	−.88330949D+04
	4	.11973492D+03	−.17612711D+04	.47891586D+04	.36861357D+04	−.28398718D+05	.28011526D+05
	5	.26809227D+01	.20193211D+04	−.77687409D+04	.24909938D+04	.25959276D+05	−.30557741D+05
	6	−.41865808D+02	−.80104226D+03	.37256750D+04	−.29538223D+04	−.81843850D+04	.11438708D+05

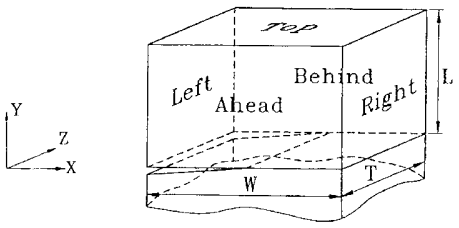

Fig. 5 Configurations of a rectangular cracked body with an edge through crack

symmetry, there are only five boundaries, i.e., top side, right side, left side, ahead side and behind side should be analyzed and the corresponding configurations are shown in Fig. 5. The tabulation of these coefficients given in Tables 1 and 2 are found to provide accurate representations of numerical results. Figures 6a to 6e represent the boundary weight functions of through crack for major contribution of the stress intensity factor in each side. In these figures, the actual nodal weight functions obtained from finite element analysis are represented by discrete points, and those calculated from the fitted nodal weight functions are plotted as solid lines. The accuracy of the predicted weight functions are checked directly against the finite element results. Excellent agreement between the two results are shown in these figures and this indicates that the fitted weight functions are good approximations to the actual finite element numerical results. The error that results from the process of curve fitting by means of the least squares method is less than 1% in general. The boundary weight functions are all smooth curves and no singular behavior will occur.

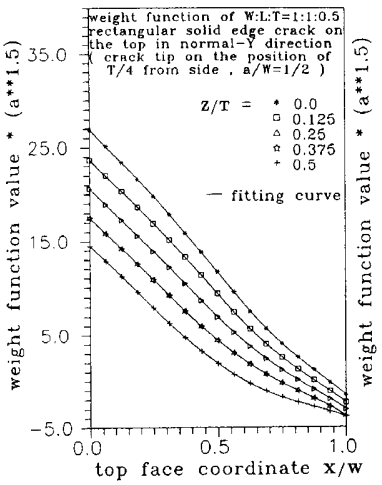

Fig. 6a Boundary weight function for an edge through crack subjected to normal loading (*Y*-direction) in the top face

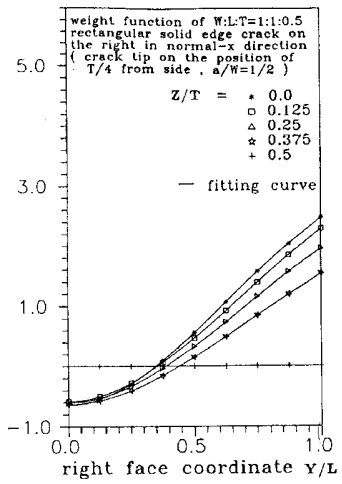

Fig. 6b Boundary weight function for an edge through crack subjected to normal loading (*X*-direction) in the right face

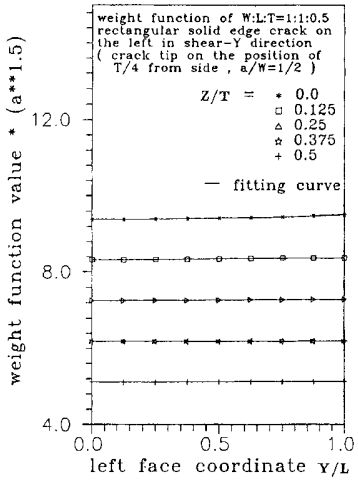

Fig. 6c Boundary weight function for an edge through crack subjected to shear loading (*Y*-direction) in the left face

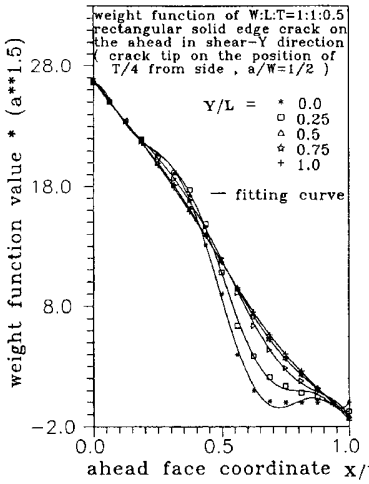

Fig. 6d Boundary weight function for an edge through crack subjected to shear loading (*Y*-direction) in the ahead face

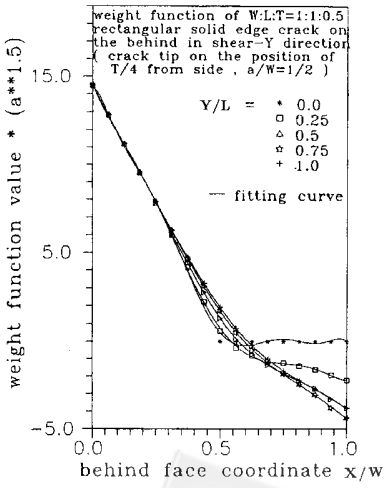

Fig. 6e Boundary weight function for an edge through crack subjected to shear loading (*Y*-direction) in the behind face

These predetermined explicit weight functions as expressed in (9) for finite rectangular cracked body along the boundaries are ready to use to evaluate the stress intensity factors for arbitrary cracked geometries. The procedure is rather simple, the first step is to evaluate the stress distribution inside the arbitrary cracked geometry along the cut rectangular boundaries. Since the rectangular boundary is far away from the crack tip, it will have no difficulty in obtaining good numerical result for stress distribution along the cut rectangular boundaries. The next step is to combine the predetermined weight function (Eq. (9) and Tables 1 and 2) and the obtained stress distribution along the cut rectangular boundaries, accurate stress intensity factors can be evaluated by a simple integration according to (8). In order to demonstrate the accuracy and validity of the boundary weight functions obtained in this paper in determining the stress intensity factors, several crack geometries have been considered and the results will be compared with the findings of earlier studies. We first consider the case that a rectangular body contains an edge through crack and subjected to a uniformly distributed line loading applied at the edge of the top faces. The mode I stress intensity factor are shown in Fig. 7, since there is no previous result available, finite element computations were made to evaluate the stress intensity factor and the results compare very well with the solutions calculated from the weight function method. The stress intensity factors from finite element calculations are obtained by using the nodal-force method, the details of which are given in [17]. It is also shown in this figure that the stress intensity factor near the center of the crack front line (i.e., $Z/T = 0.5$) for thick body (i.e., $T/W = 1$) is very close to the result evaluated by two dimensional plane strain condition. The next case is a rectangular body containing an edge through crack of length a, is subjected to a uniformly distributed tensile stress at the top surface. The results of the stress intensity factor are shown in Fig. 8 and are compared with the finite element solutions. Figure 8 also shows the stress intensity factor (thick lines) evaluated by using the finite element method based on two-dimensional plane stress formulation. The state of stress varies from plane strain in the interior to plane stress at the free surface. We can see that the two-dimensional plane stress formulation is underestimated the stress intensity factor for three-dimensional bodies. Comparison of the stress intensity factors calculated by using the above proposed boundary weight functions with the results obtained by others revealed satisfactory accuracy and validity of the boundary weight function method.

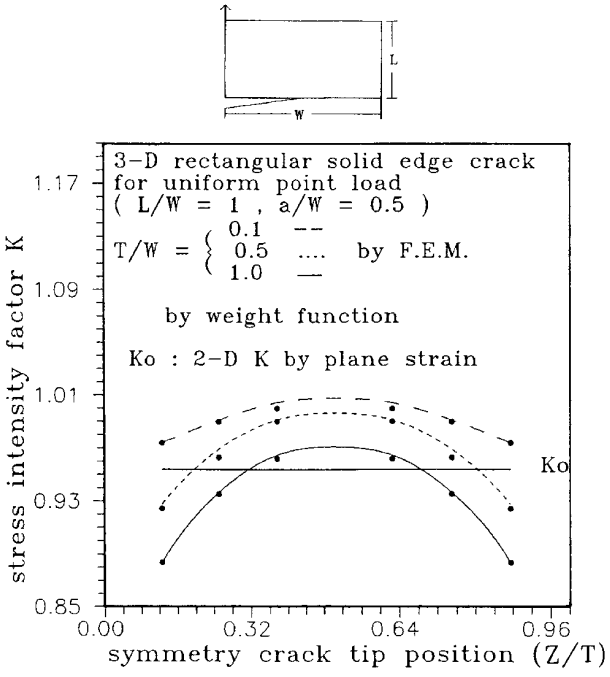

Fig. 7 Mode I stress intensity factors calculated from the bondary weight function method and finite element method for an edge through crack subjected to uniformly distributed line loadings applied at the edge of top faces

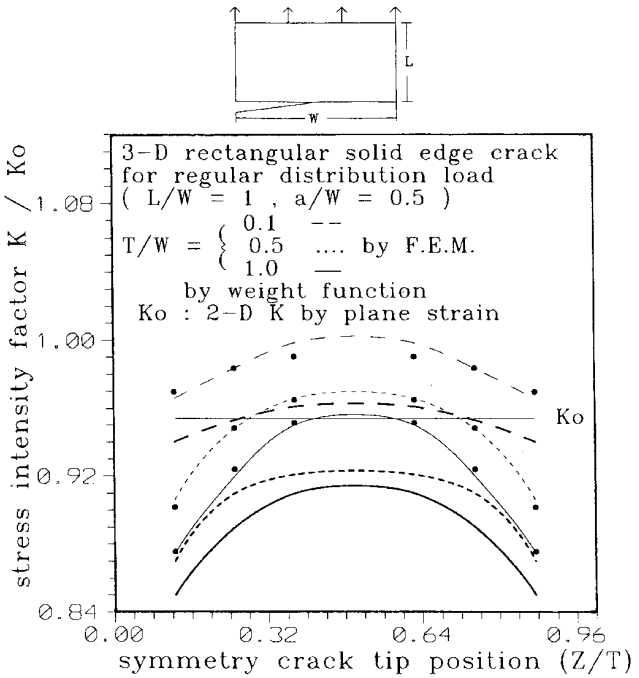

Fig. 8 Mode I stress intensity factors calculated from the boundary weight function method and finite element method for an edge through crack subjected to uniformly distributed loadings at top faces

4. CONCLUSIONS

The methods of calculating stress intensity factors based on weight function techniques are efficient and economical, since once the weight function is determined for a given crack geometry, the stress intensity factor for any loading condition can be obtained by a simple integration. For the conventional

study on weight function, most investigations are done for the crack face weight function which is usually suitable for a given geometry of cracked bodies. The aim of this manuscript is to present a weight function formulation which will allow calculation of the stress intensity factor from an integral on fixed boundaries within the body. This is in contrast to what many researches have done in the past in which the weight function has been calculated on the crack faces in two-dimensions or crack surfaces in three-dimensions. In this study, the boundary weight function concept has proposed to calculate the stress intensity factors for arbitrary shape of cracked geometries in three dimensional case and subjected to general boundary conditions. Hence the boundary weight function method is more useful in practical applications. The simplest loading condition of uniform tension and an efficient finite element methodology has been achieved for evaluating the boundary weight functions for rectangular cracked bodies. In order to facilitate the utilization of the discretized nodal boundary weight functions, they are expressed in a general polynomial form whose parameters are determined by a least square fitting of the finite element results for rectangular cracked body. These empirical equations for the boundary weight functions of rectangular cracked body have been successful obtained in this study. The stress intensity factors of cracked bodies subjected to arbitrary applied loadings can be obtained very efficiently by combining the stress field on the boundaries of cut rectangular cracked body with the interpolated boundary weight functions. Very satisfactory results of the stress intensity factors are obtained by the proposed boundary weight function method when compared to known solutions of other workers.

ACKNOWLEDGEMENT

This research support of the Republic of China Natioanl Science Council through Grant NSC80-0210-D002-32 at National Taiwan University is gratefully acknowledged.

REFERENCES

1. Tada, H., Paris, P. C. and Irwan, G. R., *The Stress Analysis of Cracks Handbook*, Del Research Corporation, Hellertown, Penna (1973).
2. Rooke, D. P. and Cartwright, D. J., *Compendium of Stress Intensity Factors*, Her Majesty's Stationery Office, London (1976).
3. Sih, G. C., *Handbook of Stress Intensity Factors*, Institute of Fracture and Solid Mechanics, Lehigh University (1973).
4. Bueckner, H. F., "A Novel Principle for the Computation of Stress Intensity Factor," *ZAMM*, Vol. 50, pp. 529–546 (1970).
5. Rice, J. R., "Some Remarks on Elastic Crack-tip Stress Fields," *International Journal of Solids and Structures*, Vol. 8, pp. 751–758 (1972)..
6. Bowie, O. L. and Freese, C. E., "Cracked-Rectangular Sheet with Linerly Varying End Displacements," *Engineering Fracture Mechanics*, Vol. 14, pp. 519–526 (1981).
7. Bortman, Y. and Banks-Sills, L., "An Extended Weight Function Method for Mixed-mode Elastic Crack Analysis," *Jounral of Applied Mechanics*, Vol. 50, pp. 907–909 (1983).
8. Sha, G. T., "Stiffness Derivatives Finite Element Technique to Determine Nodal Weight Functions with Singularity Elements," *Engineering Fracture Mechanics*, Vol. 19, pp. 685–699 (1984).
9. Sha, G. T. and Yang, C. T., "Weight Function Calculations for Mixed-mode Fracture Problems with the Virtual Crack Extension Technique," *Engineering Fracture Mechanics*, Vol. 21, pp. 1119–1149 (1985).
10. Parks, D. M., "A Stiffness Derivative Finite Element Technique for Determination of Crack Tip Stress Intensity Factors," *International Journal of Fracture*, Vol. 10, pp. 487–501 (1974).
11. Hellen, T. K. "On the Method of Virtual Crack Extensions," *International Journal of Numerical Methods in Engineering*, Vol. 9, pp. 187–207 (1975).
12. Tsai, C. H. and Ma, C. C., "Weight Functions for Cracks in Finite Rectangular Plates," *International Journal of Fracture*, Vol. 40, pp. 43–63 (1989).
13. Ma, C. C., Chang, Z. and Tsai, C. H., "Weight Functions of Oblique Edge and Center Cracks in Finite Bodies," *Engineering Fracture Mechanics*, Vol. 36, pp. 267–285 (1990).
14. Ishikawa, H., "A Finite Element Analysis of Stress Intensity Factors for Combined Tensile and Shear Loading by Only a Virtual Crack Extension," *International Journal of Fracture*, Vol. 16, pp. 243–246 (1980).
15. Sha, G. T., "On the Virtual Crack Extension Technique for Stress Intensity Factors and Energy Release Rate Calculations for Mixed Fracture Mode," *International Journal of Fracture*, Vol. 25, pp. R33–42 (1984).
16. Banks-Sills, L. and Makevet, L., "A Numerical Mode I Weight Function for Calculating Stress Intensity Factors of Three-Dimensional Cracked Bodies," *International Journal of Fracture*, Vol. 76, pp. 169–191 (1996).
17. Raju, I. S. and Newman, Jr. J. C., "Stress Intensity Factor for a Wide Range of Semi-Elliptical Surface Cracks in Finite-Thickness Plates," *Engineering Fracture Mechanics*, Vol. 11, pp. 817–829 (1979).
18. Heckmer, J. L. and Bloom, J. M., "Determination of Stress Intensity Factors for the Corner-Cracked Hole

Using the Isoparametric Singularity Element," *International Journal of Fracture*, Vol. 13, pp. 732–736 (1977).

19. Ma, C. C., Shen, I. K. and Tsai, P., "Calculation of the Stress Intensity Factor for Arbitrary Finite Cracked Body by Using the Boundary Weight Function Method," *International Journal of Fracture*, Vol. 70, pp. 183–202 (1995).
20. Labbens, R. C., Heliot, J. and Pellissier-Tanon, A., "Weight Function for Three-Dimensional Symmetrical Crack Problems," *ASTM STP*, Vol. 601, pp. 448–470 (1976).

(Manuscript received Dec. 18, 1998,
Accepted for publication Jan. 7, 1999.)